

# Supporting information

## Hydrazine N-N Bond Cleavage over Silica-Supported Tantalum

### Hydrides

Hong-Peng Jia,<sup>a,†</sup> Eric Gouré,<sup>a,§</sup> Xavier Solans-Monfort,<sup>b,\*</sup> Jessica Llop Castelbou,<sup>a</sup>  
Catherine Chow,<sup>a,‡</sup> Mostafa Taoufik,<sup>a</sup> Odile Eisenstein,<sup>c,\*</sup> Elsje Alessandra Quadrelli<sup>a,\*</sup>

#### Adresses

a) Laboratoire C2P2 (équipe COMS), UMR 5265 CNRS- Université de Lyon 1 - CPE  
Lyon, 43, Bvd du 11 Novembre 1918, 69616 Villeurbanne, France.

b) Departament de Química, Universitat Autònoma de Barcelona, 08193 Bellaterra,  
Spain.

c) Institut Charles Gerhardt, UMR 5253 CNRS Université de Montpellier, cc 1501,  
Place E. Bataillon, 34095 Montpellier, France.

#### *Present addresses:*

<sup>†</sup>*Institute of Urban Environment, Chinese Academy of Sciences, 1799 Jimei Road,  
Xiamen, 361021 China.*

<sup>§</sup>*DMC/CIRE – UMR 5250 CNRS-UJF, ICMG FR-2607 - Université Joseph Fourier -  
Grenoble 1.*

<sup>‡</sup>*The University of British Columbia, Department of Chemistry, 2036 Main Mall,  
Vancouver, Canada V6T 1Z1.*

## TABLE OF CONTENTS

<b>Experimental Details</b>	<b>S3-S5</b>
<b>Table S1.</b>	<b>S6</b>
<b>Table S2.</b>	<b>S7</b>
<b>Figure S1.</b>	<b>S8</b>
<b>Figure S2.</b>	<b>S9</b>
<b>Figure S3.</b>	<b>S10</b>
<b>Figure S4.</b>	<b>S11</b>
<b>Figure S5:</b>	<b>S12</b>
<b>Figure S6.</b>	<b>S13</b>
<b>Figure S7.</b>	<b>S14</b>
<b>Figure S8.</b>	<b>S15</b>
<b>Figure S9.</b>	<b>S16</b>
<b>References</b>	<b>S17</b>

## Experimental Details

All experiments were carried out by using standard air-free methodology in an argon-filled Vacuum Atmospheres glovebox, on a Schlenk line or in a Schlenk-type apparatus interfaced to a high-vacuum line ( $10^{-5}$  Torr).  $[\text{Ta}(\text{CH}_2\text{C}(\text{CH}_3)_3)_3(=\text{CHC}(\text{CH}_3)_3)]$  was commercial from STREM company without further purification. MCM-41 mesoporous silica was purchased from Sigma-Aldrich Company. MCM-41 supported tantalum hydrides  $[(\equiv\text{SiO})_2\text{TaH}]$ , **1a**, and  $[(\equiv\text{SiO})_2\text{TaH}_3]$ , **1b**, were prepared by impregnation in pentane or by sublimation for *in situ* IR monitoring as previously reported by the reaction of  $[\text{Ta}(\text{CH}_2^t\text{Bu})_3(=\text{CH}^t\text{Bu})]$  with MCM-41 previously dehydroxylated at  $500^\circ\text{C}$ , followed by hydrogenolysis (550 Torr, 15h,  $150^\circ\text{C}$ ).<sup>1</sup> Dry pentane was distilled on NaK alloy followed by degassing through three freeze-pump-thaw cycles.

*Gas-phase analysis of alkanes and  $\text{H}_2$ :* Gas phase analysis was performed on a Hewlett-Packard 5890 series II gas chromatograph equipped with a flame ionization detector and an  $\text{Al}_2\text{O}_3/\text{KCl}$  on fused silica column (50m X 0.32 mm). Dihydrogen gas phase analysis was performed on an intersmat-IGC 120-MB gas chromatograph equipped with a catharometer (TCD, thermal conductivity detector).

*Infrared spectra* were recorded on a Nicolet 550-FT spectrometer by using an infrared cell equipped with  $\text{CaF}_2$  windows, allowing *in situ* monitoring under controlled atmosphere. Typically 36 scans were accumulated for each spectrum (resolution,  $4\text{ cm}^{-1}$ ). DRIFT spectra were recorded on a Nicolet 550-FT spectrometer and sample loading was performed in argon-filled glovebox.

*Solid-state NMR spectra* were recorded on a Bruker DSX-500 spectrometer equipped with a standard 4-mm double-bearing probe head and operating at 75.47, 500, MHz for  $^{13}\text{C}$ ,  $^1\text{H}$  and  $^{15}\text{N}$  respectively.

The samples were introduced in the rotor made of zirconia in a glovebox and tightly closed. Compressed air was used for both of bearing and driving the rotors.

### Preparation of $[(\equiv\text{SiO})_2\text{TaH}]$ and $[(\equiv\text{SiO})_2\text{TaH}_3]$ , **1**:

Powder of  $[(\equiv\text{SiO})_2\text{Ta}(\text{CH}_2^t\text{Bu})(\text{CH}_2^t\text{Bu})_2]$  (500mg, 0.32 mmol Ta) was twice treated at  $150^\circ\text{C}$  with anhydrous hydrogen (600 torr, 16.4 mmol, 65 equivalent / Ta) for 15 h. Gas chromatography analysis indicated the formation of  $13\pm 2\text{ CH}_4$  coming from the hydrogenolysis of 2,2-dimethylpropane,  $\text{CMe}_4$  ( $2.6\pm 0.4\text{ CMe}_4/\text{Ta}$ , expected 3). The gas

evolved during the reaction was removed under vacuum and the final hydrides  $[(\equiv\text{SiO})_2\text{TaH}]$ , **1a**, and  $[(\equiv\text{SiO})_2\text{TaH}_3]$ , **1b**, were obtained as a brown powder. As already reported, some surface alkyl groups ( $<0.1$  C/Ta) resist hydrogenolysis. Elemental Analysis: Ta 15.91% wt C 0.67% wt. Solid state  $^1\text{H}$  MAS NMR = 29.5, 26.8, 23.2, 18.0, 13.0 (Ta(**H**)<sub>x</sub>), 4.3, 4.0 (Si**H** and Si**H**<sub>2</sub>), 1.8 (Si**OH**), 0.8 (C**H**<sub>n</sub>) ppm. IR: 3747 ( $\nu_{\text{OH}}$ ), 3270-2850 ( $\nu_{\text{CH}}$ ), 2270 ( $\nu_{\text{SiH}}$ ), 2220 ( $\nu_{\text{SiH}_2}$ ), 2100-1600 ( $\delta_{\text{Si-O-Si}}$ ), 1890-1700 ( $\nu_{\text{TaH}}$ ), 1467 w, 1362 ( $\delta_{\text{CH}}$ )  $\text{cm}^{-1}$ .

### **In-situ IR study of the reaction of $[(\equiv\text{SiO})_2\text{TaH}_x]$ , **1** with hydrazine:**

Hydrazine was prepared by the reaction of KOH with hydrazine monohydrate 64-65 %, reagent grade, 98 % (Sigma Aldrich) according to literature procedure.<sup>2</sup> Addition of  $\text{N}_2\text{H}_4$  (14.4 torr at 25 °C) on  $[(\equiv\text{SiO})_2\text{TaH}_x]$ , **1**, (25 mg, 0.025 mmol Ta) was done at room temperature and gave the following IR peaks.

Selected IR frequencies for the reaction of physisorbed  $\text{N}_2\text{H}_4$ : 3368 ( $\nu_{\text{NH}}$ ), 3290 ( $\nu_{\text{NH}}$ ), 3197 ( $\nu_{\text{NH}}$ ), 1612 ( $\delta_{\text{NH}_2}$ )  $\text{cm}^{-1}$ .

Selected IR frequencies for the reaction of  $[(\equiv\text{SiO})_2\text{TaH}_x]$  with  $\text{N}_2\text{H}_4$ : 3747 ( $\nu_{\text{OH}}$ ), 3359 ( $\nu_{\text{NH}}$ ), 3285 ( $\nu_{\text{NH}}$ ), 3190 ( $\nu_{\text{NH}}$ ), 3270-2850 ( $\nu_{\text{CH}}$ ), 2270 ( $\nu_{\text{SiH}}$ ), 2220 ( $\nu_{\text{SiH}_2}$ ), 2100-1600 ( $\delta_{\text{Si-O-Si}}$ ), 1890-1700 ( $\nu_{\text{TaH}}$ ), 1605 ( $\delta_{\text{NH}_2}$ )  $\text{cm}^{-1}$ .

Excess of the hydrazine was needed to consume the total TaH peaks and new peaks in NH region appeared with thermal-treatment at 100 °C.

Selected IR frequencies for the reaction of  $[(\equiv\text{SiO})_2\text{TaH}_x]$  with  $\text{N}_2\text{H}_4$  at 100 °C: 3747 ( $\nu_{\text{OH}}$ ), 3494 ( $\nu_{\text{NH}}$ ), 3358 ( $\nu_{\text{NH}}$ ), 3374 ( $\nu_{\text{NH}}$ ), 3294 ( $\nu_{\text{NH}}$ ), 3270-2850 ( $\nu_{\text{CH}}$ ), 2270 ( $\nu_{\text{SiH}}$ ), 2220 ( $\nu_{\text{SiH}_2}$ ), 2100-1600 ( $\delta_{\text{Si-O-Si}}$ ), 1613 ( $\delta_{\text{NH}_2}$ )  $\text{cm}^{-1}$ .

The same experiment was also done with  $[(\equiv\text{SiO})_2\text{TaH}_x]$ , **1**, (15 mg, 0.02 mmol) with  $\text{N}_2\text{H}_4$  which didn't lead to the complete consumption of TaH peaks at room temperature.

Selected IR frequencies for the reaction with  $\text{N}_2\text{H}_4$  at 150 °C: 3747 ( $\nu_{\text{OH}}$ ), 3500 ( $\nu_{\text{Ta-N-H}}$ ), 3461 ( $\nu_{\text{N-H}}$ ), 3372 ( $\nu_{\text{Ta-N-H}}$ ), 3270-2850 ( $\nu_{\text{CH}}$ ), 2270 ( $\nu_{\text{SiH}}$ ), 2220 ( $\nu_{\text{SiH}_2}$ ), 2100-1600 ( $\delta_{\text{Si-O-Si}}$ ), 1890-1700 ( $\nu_{\text{TaH}}$ ), 1520 ( $\delta_{\text{TaNH}_2}$ )  $\text{cm}^{-1}$ .

Elemental analysis: Ta 15,7 % wt; N 1,34 % wt. (N/Ta by e.a. = ca. 0.96 and 0.95).

**The reaction of  $[(\equiv\text{SiO})_2\text{TaH}_x]$ , **1** with  $^{15}\text{N}$ -labeled hydrazine:**

A disk of  $[(\equiv\text{SiO})_2\text{TaH}_x]$ , **1**, (25 mg, 0.025 mmol Ta), prepared as previously reported, was treated by  $^{15}\text{N}_2\text{H}_4$  (14.4 torr at 25 °C). Peaks in the  $\nu$  (NH) and  $\delta$  ( $\text{NH}_2$ ) region confirmed the presence of  $^{15}\text{N}$ -hydrazine on the pellet with an expected redshift.

Selected IR frequencies for the reaction with  $^{15}\text{N}_2\text{H}_4$  ( $\nu$  (NH): 3348, 3278, 3189  $\text{cm}^{-1}$ ;  $\delta$  ( $\text{NH}_2$ ): 1608  $\text{cm}^{-1}$ ).

Heating the sample at 100 °C for 2 h gave the peaks at 1516 and 1545  $\text{cm}^{-1}$  leading the Ta- $^{15}\text{NH}_2$  and Si- $^{15}\text{NH}_2$  respectively.

**Control experiment on hydrazine stability at 100°C**

To eliminate the possibility that the reaction can occur in the absence of the metal-hydride, a control experiment was carried out. Hydrazine was heated at 100 °C on tantalum-free starting silica pellet. The IR spectrum show bands at 3367, 3291, 3198 and 1612  $\text{cm}^{-1}$ , mentioned above, which are characterized of stretching  $\nu(\text{NH})_x$  and  $\delta(\text{NH}_2)$  modes of physisorbed hydrazine on pure silica (Figure S1). Physisorbed hydrazine cannot be substantially removed under dynamic vacuum treatment (1h at  $10^{-5}$  torr). The evolution of the IR spectrum with temperature shows that hydrazine starts decomposing above 150 °C, when bands at 3408 and 3322  $\text{cm}^{-1}$  start to appear (see spectrum Figure S2d). These bands were previously assigned to the stretching frequencies of ammonia physisorbed on pure silica (Figure S2e).<sup>1</sup> This control experiment indicates that hydrazine does not transform at 100 °C in the absence of tantalum complexes.

**Table S1.** Relative energies (kcal/mol) with respect to **Ib** + N<sub>2</sub>H<sub>4</sub> of products and potential reaction intermediates as function of the level of theory, basis sets and silica surface modeling (cluster vs. periodic). See Figure S6 for periodic model representation and Figures S6 to S9 for species labeling.

Species	M06/ aug-cc-pVDZ	PBE-D3/ aug-cc-pVDZ	PBE-D3/ DZVP	Periodic
<b>Ia</b>	40.0	45.4	45.2	46.1
<b>Ib</b>	0.0	0.0	0.0	0.0
<b>Ib-N<sub>2</sub>H<sub>4</sub>-mer</b>	-29.9	-29.5	-29.1	-37.4
<b>Ib-N<sub>2</sub>H<sub>4</sub>-fac</b>	-25.6	-23.9	-24.2	-28.6
<b>Ib-<math>\eta^1</math>-N<sub>2</sub>H<sub>4</sub></b>	-24.8	-24.1	-25.4	-27.3
<b>II</b>	-76.3	-71.9	-81.3	-82.0
<b>III</b>	-87.6	-82.6	-89.2	-91.7
<b>IV-eq</b>	-31.6	-29.5	-33.4	-34.7
<b>IV-cis</b>	-30.4	-28.0	-31.9	-33.0
<b>V-Is1</b>	-88.6	-85.0	-88.9	-91.4
<b>V-Is2</b>	-86.2	-81.9	-86.4	-94.5

**Table S2.** Differences in the relative energies (in kcal/mol) with respect to **Ib** + N<sub>2</sub>H<sub>4</sub> of products and intermediates as function of: a) level of theory, b) basis sets and c) surface modeling. See Figure S6 for periodic model representation and Figures S7 to S9 for species labeling.

Species	$\Delta E_{\text{functional}}^{\text{a}}$	$\Delta E_{\text{basis}}^{\text{b}}$	$\Delta E_{\text{model}}^{\text{c}}$
<b>Ia</b>	-5.4	-0.2	+0.9
<b>Ib</b>	--	--	--
<b>Ib-N<sub>2</sub>H<sub>4</sub>-mer</b>	-0.4	+0.4	-8.3
<b>Ib-N<sub>2</sub>H<sub>4</sub>-fac</b>	-1.7	-0.3	-4.4
<b>Ib-<math>\eta^1</math>-N<sub>2</sub>H<sub>4</sub></b>	-0.7	-1.3	-1.9
<b>II</b>	-4.4	-9.3	-0.7
<b>III</b>	-5.0	-6.6	-2.5
<b>IV-eq</b>	-2.1	-3.9	-1.3
<b>IV-cis</b>	-2.4	-3.9	-1.1
<b>V-Is1</b>	-3.6	-3.9	-2.5
<b>V-Is2</b>	-4.3	-4.5	-8.1

<sup>a</sup> Energy difference between the M06/aug-cc-pDVZ and PBE-D3/aug-cc-pDVZ calculations. A positive value indicates that M06 predicts a more stable intermediate with respect to **Ib** + N<sub>2</sub>H<sub>4</sub> reactants asymptote.

<sup>b</sup> Energy difference between the PBE-D3/aug-cc-pDVZ and PBE-D3/DZVP calculations. A positive value indicates that aug-cc-pDVZ predicts a more stable intermediate with respect to **Ib** + N<sub>2</sub>H<sub>4</sub> reactants asymptote.

<sup>c</sup> Energy difference between the cluster and the periodic models using the same PBE-D3/DZVP methodology. A positive value indicates that the cluster model predicts a more stable intermediate with respect to **Ib** + N<sub>2</sub>H<sub>4</sub> reactants asymptote.

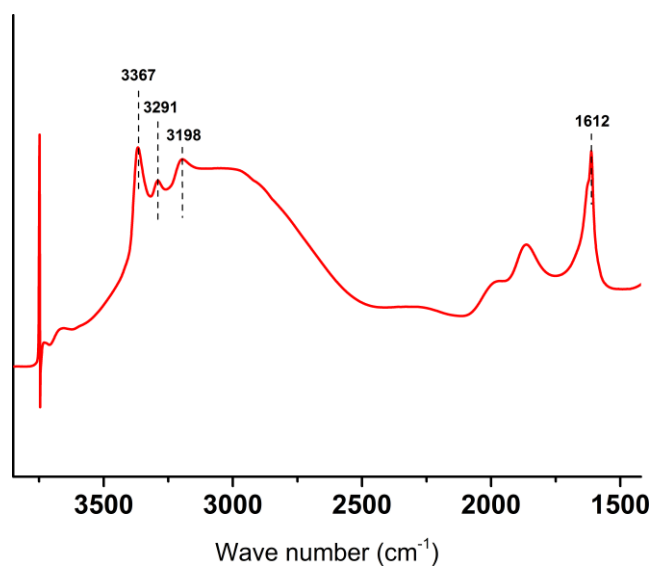


**Figure S1.** Infrared spectrum after hydrazine addition on MCM-41 pellet at room temperature.



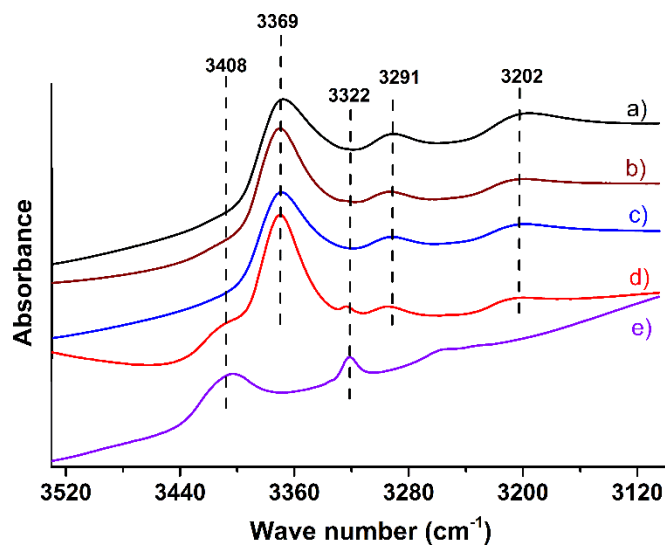


**Figure S2.** The evolution of the IR spectra between 3520 and 3120  $\text{cm}^{-1}$  of a MCM-41 pellet (ca. 25 mg, pretreated under vacuum at 500°C for 15 h) either in the presence of hydrazine (a) at room temperature (b) after 1 h at 50°C (c) after 1 h at 100°C (d) after 1 h at 150°C or (e) in the presence of ammonia at room temperature.

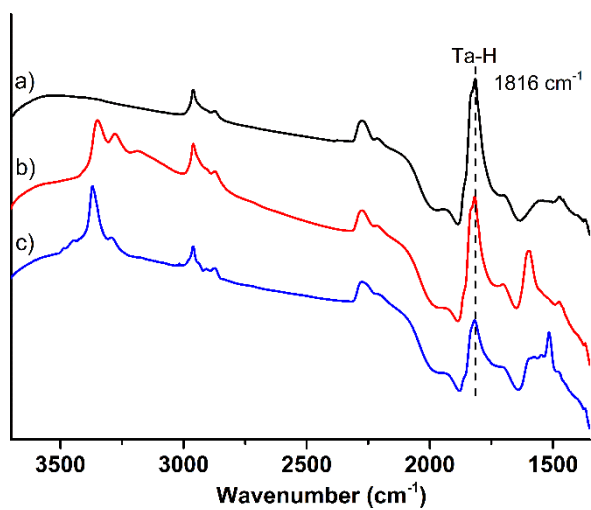


**Figure S3.** Difference IR spectra for (a) starting tantalum hydrides  $[(\equiv\text{SiO})_2\text{TaH}_x \text{ x: 1, 3}]$  (b) after addition of  $^{15}\text{N}_2\text{H}_4$  for 1h at RT (followed by gas-phase evacuation) (c) after 2h at  $100^\circ\text{C}$ . Spectrum of Starting unfunctionalized MCM-41 silica subtracted in all cases (ca. 25 mg, pretreated under vacuum at  $500^\circ\text{C}$  for 15 h). Original spectra before subtraction are reported in Figure 2 of the manuscript.

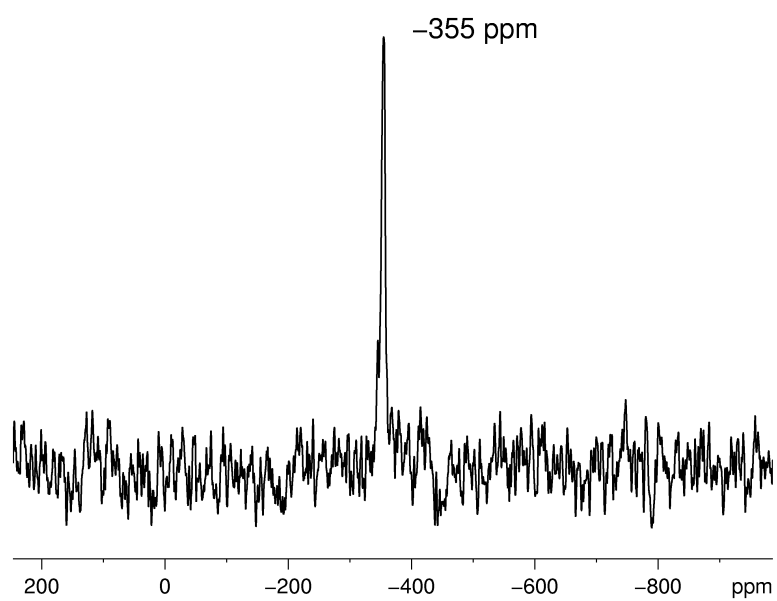
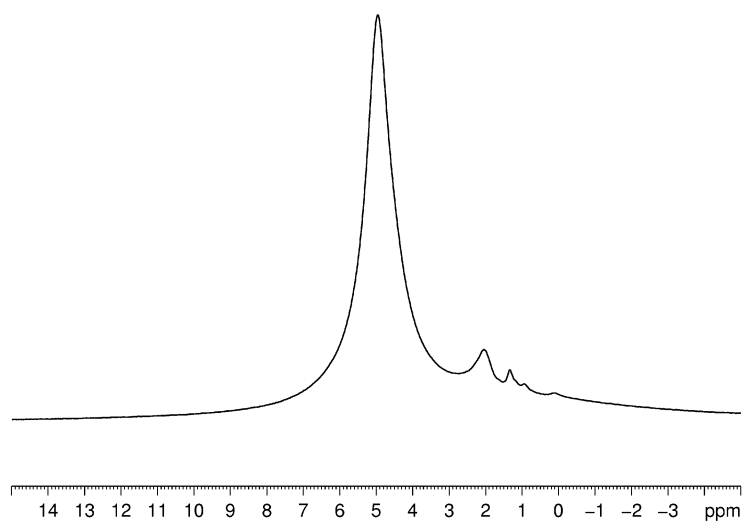


**Figure S4.** MAS SS  $^1\text{H}$ -NMR (above) and CP  $^{15}\text{N}$  NMR (below) spectra of  $\text{N}_2\text{H}_4$  physisorbed on silica pellet (MCM-41 previously dehydroxylated at 500 °C).

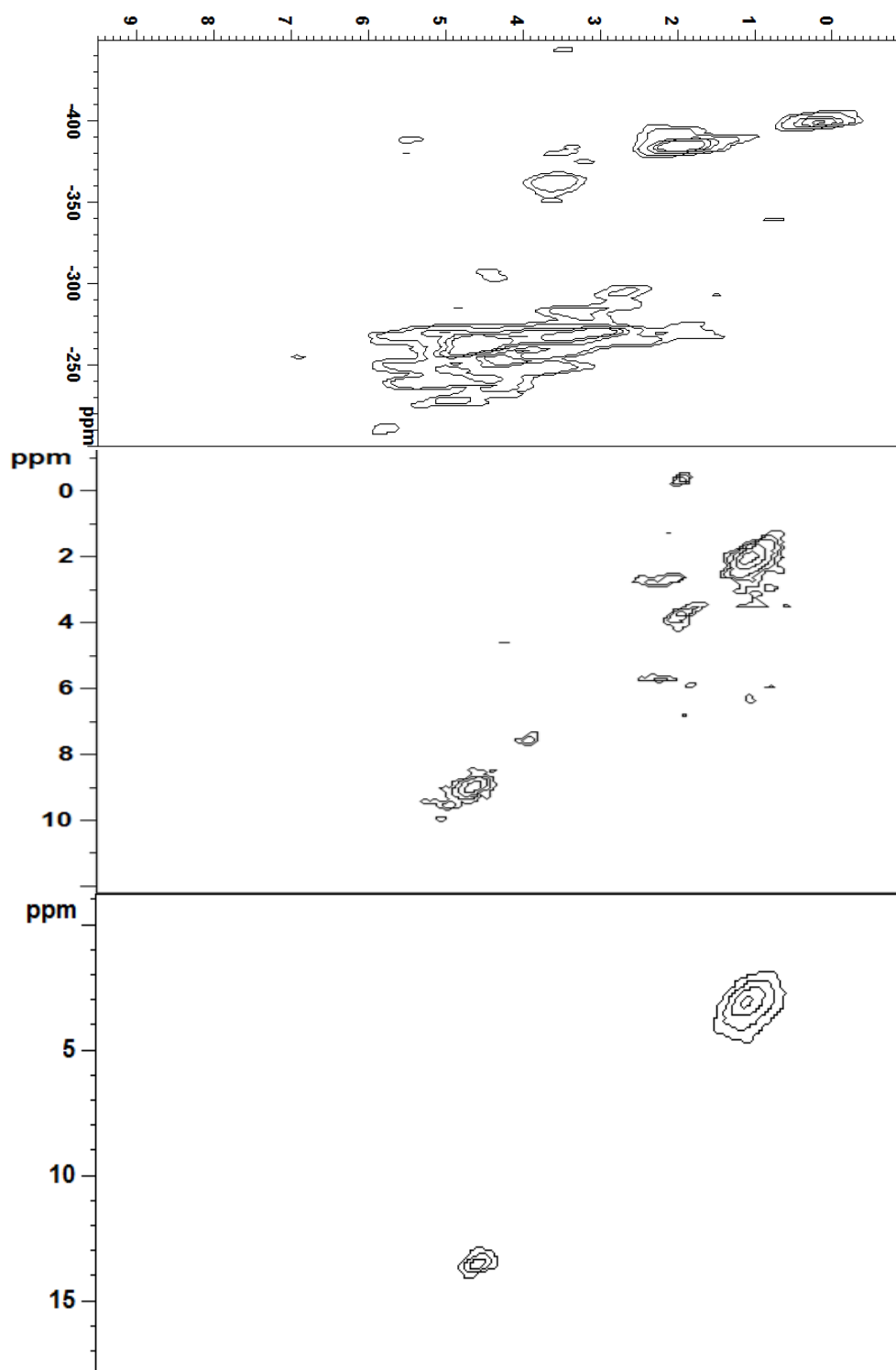


**Figure S5:** Enlarged Two-dimensional solid-state MAS correlation spectra reported in Figure 4 of manuscript.

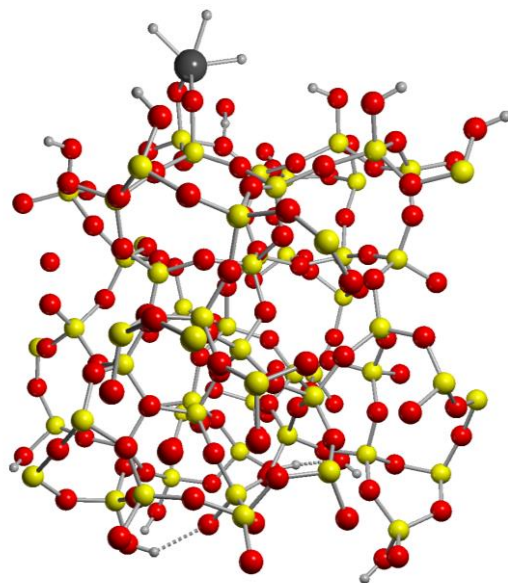


**Figure S6.** Unit cell of Periodic model

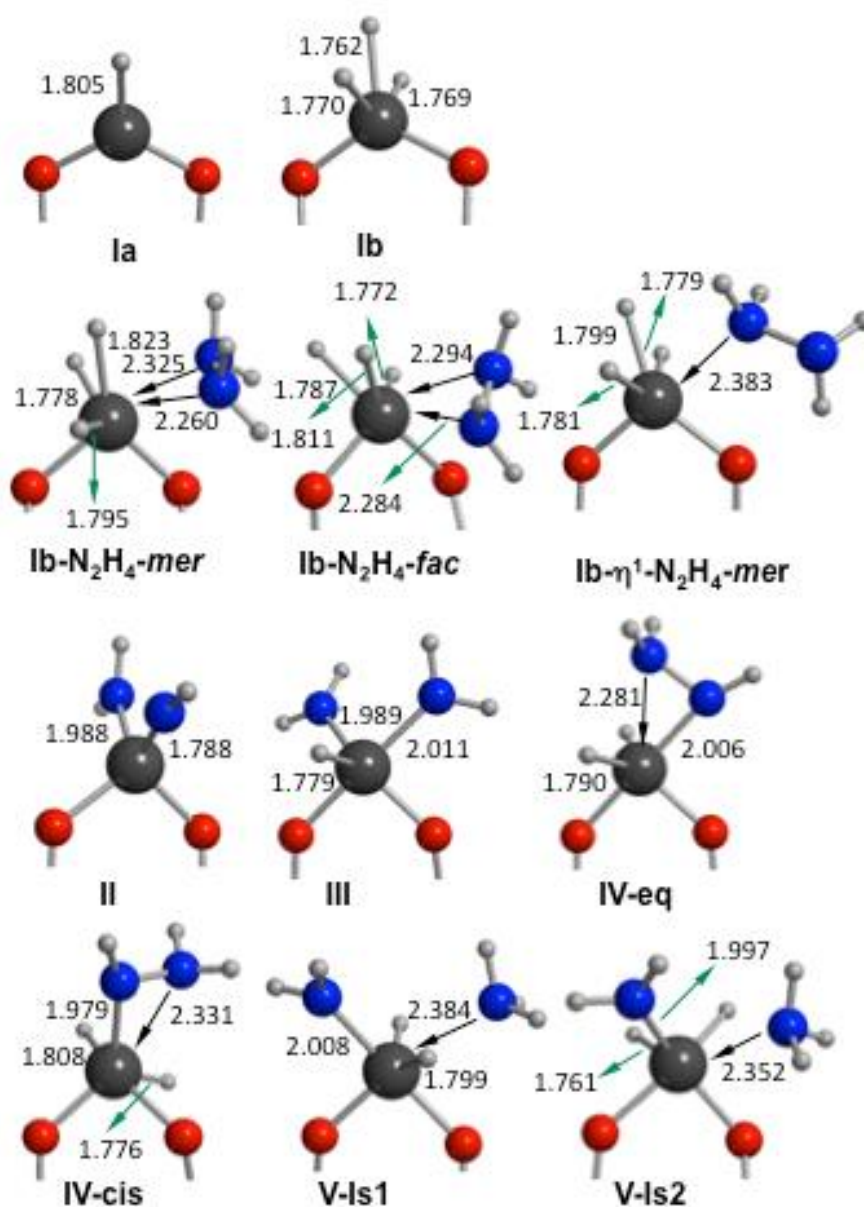


**Figure S7.** Structures and selected distances in Å for all intermediates involved in the reaction of  $\text{N}_2\text{H}_4$  with **1b**. Geometries were obtained with the cluster model of the silica surface, the PBE-D level of theory and the basis sets, we used for the Gaussian09 calculations (see computational details section). Black arrows are used for formal donor – acceptor interactions and green arrows for distances.

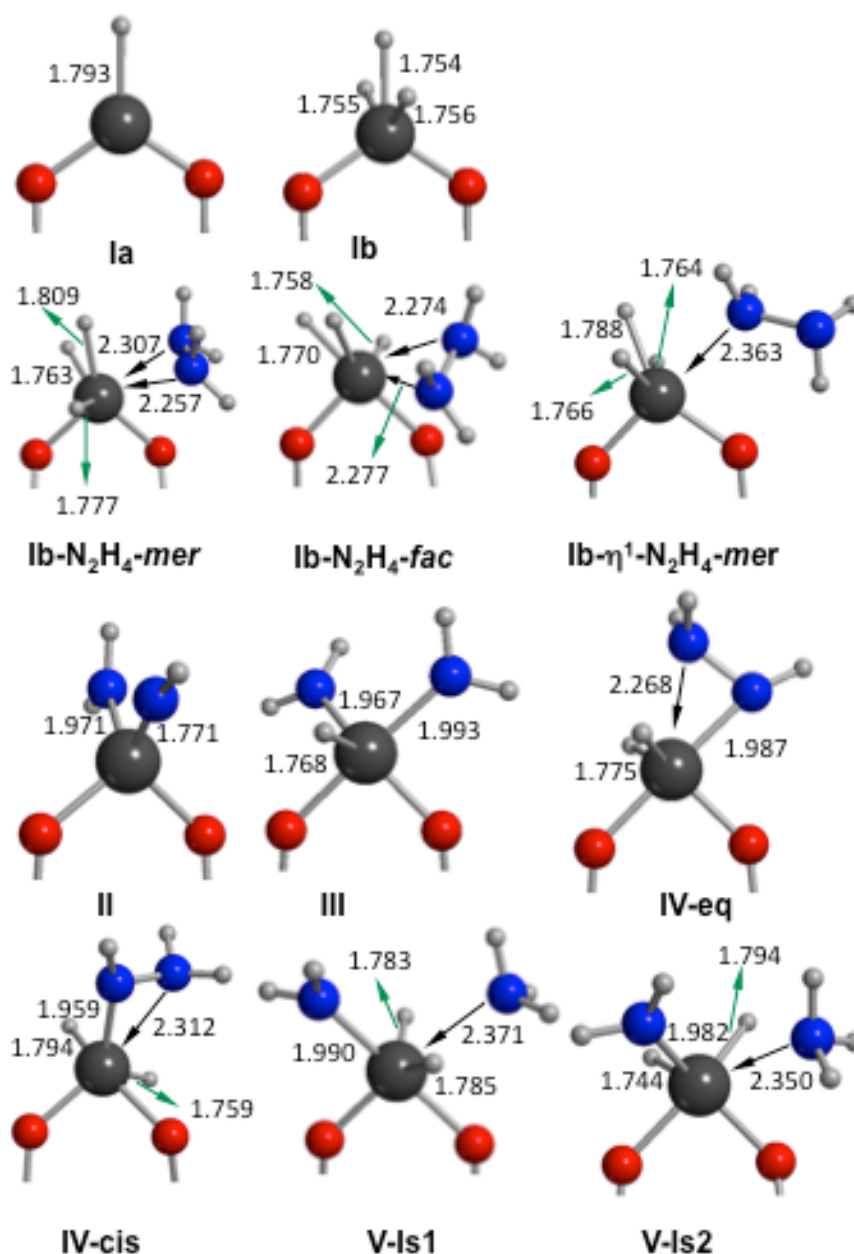


**Figure S8.** Structures and selected distances in Å for all intermediates involved in the reaction of  $\text{N}_2\text{H}_4$  with **1b**. Geometries were obtained with a cluster model of the silica surface inside of a  $40 \times 40 \times 40 \text{ Å}$  unit cell, the PBE-D level of theory and the basis sets we used for the CP2K calculations (see computational details section). Black arrows are used for formal donor – acceptor interactions and green arrows for distances.

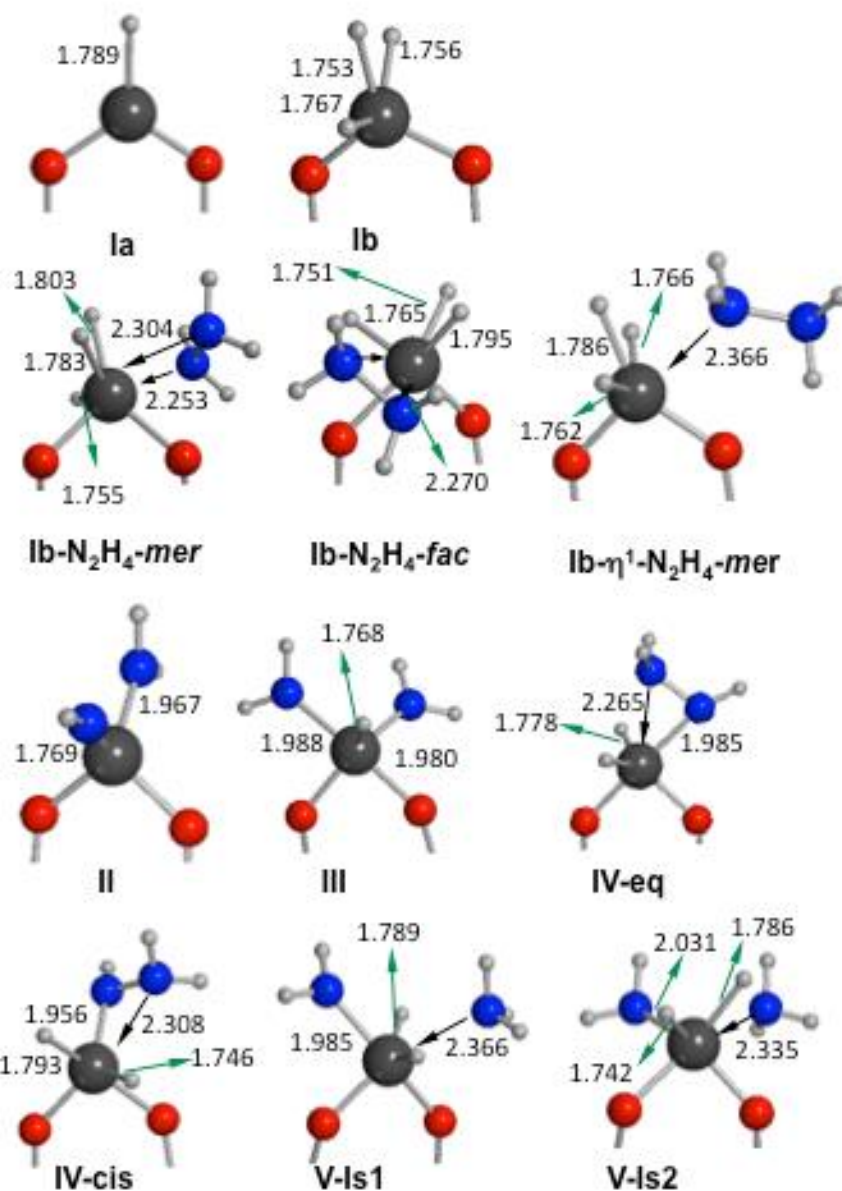


**Figure S9.** Structures and selected distances in Å for all intermediates involved in the reaction of  $\text{N}_2\text{H}_4$  with **1b**. Geometries were obtained with the periodic model of the silica surface, the PBE-D level of theory and the basis sets we used for the CP2K calculations (see computational details section). Black arrows are used for formal donor – acceptor interactions and green arrows for distances.



## References:

1. Avenier, P.; Taoufik, M.; Lesage, A.; Solans-Monfort, X.; Baudouin, A.; de Mallmann, A.; Veyre, L.; Basset, J.-M.; Eisenstein, O.; Emsley, L.; Quadrelli, E. *A. Science* **2007**, *317*, 1056–1060.
2. Hale, C. F. ; Shetterly, F. F. *J. Amer. Chem. Soc.* **1911**, *33*, 1071-1076.